Detection and assignment of ozone bands near 95% of the dissociation threshold

Semen Vasilchenko, Alain Barbe, Evgeniya Starikova, Samir Kassi, Didier Mondelain, Alain Campargue, Vladimir Tyuterev

Detection and assignment of ozone bands near 95% of the dissociation threshold

Semen Vasilchenko,[1,3] Alain Barbe,[2] Evgeniya Starikova,[1,3] Samir Kassi,[4] Didier Mondelain,[4] Alain Campargue,[4,*] and Vladimir Tyuterev[3,2]

[1]*V. E. Zuev Institute of Atmospheric Optics SB RAS, av. 1, Akademician Zuev square, 634055 Tomsk, Russia*

[2]*Groupe de Spectrométrie Moléculaire et Atmosphérique, UMR CNRS 7331, UFR Sciences Exactes et Naturelles, BP 1039 - 51687 Reims Cedex 2, France*

[3]*Laboratory of Quantum Mechanics of Molecules and Radiative Processes, Tomsk State University, 36 Lenin Avenue, 634050 Tomsk, Russia*

[4] *Université Grenoble Alpes, CNRS, LIPhy, 38000 Grenoble, France*

Various physical and chemical processes involving ozone formation and depletion remain to be understood in our atmosphere. This is the case of the mass-independent enrichment of heavy ozone isotopes in the stratosphere. The modelling of such phenomena based on ozone dynamics calculations requires a detailed knowledge the ozone potential energy surface (PES) near the dissociation threshold, D_0. Highly excited quantum states at energies approaching D_0 provide an ideal probe of PESs computed by *ab initio* methods but their detection by absorption spectroscopy is particularly challenging due to the sharp decrease of the intensity with the energy of the corresponding vibrational combination and overtone bands. In this work, two very high energy vibrational bands are detected by high sensitivity cavity ring down spectroscopy providing a noise equivalent absorption, α_{min}, on the order of a few 10^{-11} cm^{-1}. The corresponding bands, assigned to the $\nu_1+6\nu_2+3\nu_3$ and $6\nu_1+\nu_2+\nu_3$ bands centered at 7969 and 7993 cm^{-1}, respectively, are about nine orders of magnitude less intense than the well-known ν_3 fundamental near 10 µm. The (163) and (611) upper vibrational levels are the most excited levels measured so far by absorption spectroscopy. The spectrum analysis allowed for the experimental determination of 240 of their rotational levels. Their energy ranges between 93.1 and 96.6 % of the dissociation threshold. The line positions and line intensity of the two bands were modelled using the effective operator approach. Synthetic line lists of the transitions are provided with line positions empirically corrected according to the experimental value of the upper energy levels and line intensities computed using fitted parameter values of the effective dipole moment. The fitted values of the band centres and rotational constants show a very good agreement with variational predictions based on an *ab initio* potential energy surface. Recent results indicate that if the calculations are not constrained to bound levels within one potential well, they give rise to three identical potential wells separated by barriers leading to deviations of some of the energy level values predicted by the 1-well and 3-well approaches, near the dissociation threshold. A better agreement of the (163) experimentally determined energy value with the 3-well predicted value is tentatively interpreted as an evidence of the 3-well effect.

* alain.campargue@univ-grenoble-alpes.fr

I. INTRODUCTION

Various physical and chemical processes involved in the formation and depletion of ozone in the atmosphere have attracted attention over the years [1-13]. In this context, several aspects of the ozone dynamics remain to be understood for an accurate modeling at the molecular level. This concerns in particular, the knowledge of the highly excited quantum states and associated transition probabilities, near the dissociation threshold, D_0. These excited states have attracted increasing interest in various fields, in particular for a reliable interpretation of satellite measurements of the ozone absorption/emission in the upper atmosphere [14-16] in non-local thermodynamic equilibrium (non-LTE) conditions [17,18].

These are challenging tasks both for experiments and theory because of the complicated electronic structure of this unstable molecule [19-29]. Many related aspects, which are of interest for fundamental molecular physics, would benefit from extended experimental information. Among them, there are issues related to possible tunneling between potential wells [30,31], non-adiabatic coupling with excited electronic states [20-22,29], isotopic exchange reactions [32-36], unusual properties related to isotopic anomalies of the ozone formation [11,37,38], which are not yet fully understood at the molecular level.

Environmental applications and climate research impact were incentive for many laboratory studies of high-resolution spectra of ozone isotopic species ([39-47] and references therein). The most relevant information concerning absorption spectra is included in the HITRAN [48] and GEISA spectroscopic databases [49] and collected in the web-accessible information system "Spectroscopy & Molecular Properties of Ozone" (SMPO) [50].

Most of spectra in the infra-red ranging from fundamental to relatively strong overtone and combination bands with low and moderate vibration excitation are accessible by Fourier Transform spectroscopy (FTS) [39-41,50]. In terms of normal mode quantum numbers, v_i, this was limited to $\sum_i v_i \leq 6$ *i. e.* to band centers below 5600 cm^{-1} ($v_{i=1-3}$ are the conventional vibrational normal modes quantum numbers corresponding to the symmetric stretching, bending and antisymmetric stretching modes, respectively. The corresponding fundamental wavenumbers are about 1103, 701 and 1042 cm^{-1}, respectively). Due to the rapid decrease of absorption intensities of the vibrational bands at increasing wavenumbers (see Fig 2 of Ref. [52]), the FTS technique does not provide the required sensitivity to access vibrational levels approaching the dissociation threshold, D_0, evaluated around 8560 cm^{-1} (as cited in [23,26]) from thermochemical measurements by Ruscic *et al*. [51]. Highly sensitive laser techniques are required to probe states approaching D_0 [53-64]. In a series of previous works by cavity-ring-down spectroscopy (CRDS), we investigated systematically the 5850-7920 cm^{-1} spectral region [54-64]. More than thirty vibrational bands of $^{16}O_3$ were rovibrationally assigned and modelled using the effective Hamiltonian approach. The analyses of the corresponding bands provided a set of more than 5000 rovibrational levels. Their comparison with *ab initio* potential energy surfaces (PES) [26] gave new experimental insight [52] into the long-standing "reef structure" issue [19,25-27,34-36] of the PES shape in the transition state.

In the present work, improved performances of the used CRDS setup (routine noise equivalent absorption, α_{min}, on the order of a few 10^{-11} cm^{-1}) allowed for extending the measurements above 7920 cm^{-1} and for the detection the most excited absorption bands of ozone reported so far. In particular, the highest energy level determined from the analysis is only 3% below the dissociation threshold. The rest of the paper is structured as follows. The experimental work, including spectrometer and measurement of line parameters, is described in Section II. Section III is devoted to the assignment of the observed lines, band analyses, determination of rovibrational energies and effective dipole moments. The discussion (Section IV) includes a comparison with *ab initio* predictions.

II. EXPERIMENT

Compared to our previous CRDS studies of ozone below 7920 cm^{-1} [54-65], the present use of an external cavity diode laser (ECDL) instead of a series of fibered distributed feedback (DFB) allows for a more efficient light injection into the CRDS cell and thus for an improved sensitivity. These improved performances are necessary to detect the extremely weak ozone bands located around 8000 cm^{-1}. The same setup was recently used to characterize the high energy part of the O_2 band at 1.27 µm [65] and extremely weak transitions in the 1.18 µm window of CO_2 [66]. From recordings with noise equivalent absorption, α_{min}, on the order of a few 10^{-12} cm^{-1}, lines among the weakest ever reported (intensity as low as 5×10^{-31} cm/molecule) could be measured [65,66]. In the following we recall the different parts of the setup and the procedure adopted for the recording of the ozone spectra.

A. The CW-CRDS spectrometer

The heart of the spectrometer is a high-finesse optical resonator made of a stainless tube fitted with two highly reflective mirrors on its extremities, one of them being mounted on a piezo electric element (PEE) PEE_C, that allows the cavity length to be slightly length-modulated. To limit the gas temperature gradients, this sample cell was covered with a tube of insulation foam and placed inside a plexiglas enclosure in order. The stainless tube temperature was continuously monitored with an analogue temperature sensor (TSic 501, IST-AG, ±0.1 K accuracy). The sample pressure, in the cell, was continuously monitored with a 1000 Torr capacitance gauge (MKS Baratron, 0.15% accuracy of the reading). During the various days of the measurement campain the temperature varied between 293.8 and 294.1 K.

The reader is referred to Konefal *et al.* (in particular its Fig. 2) [65] for a detailed description of the CRDS set-up, except that, in sake of a faster scan rate, we did not implement the optical frequency comb referencing or disciplining. Briefly, the ECDL light is first sent into a polarization maintained fiber coupler (PFC, 90/10), which directs about 10% of the emitted light to a Fizeau wavemeter (High Finesse WS-U-30 IR, 5 MHz resolution, 20 MHz accuracy) and the remaining 90% into a fibered acousto-optic modulator (AOM) inserted before the 1.4-meter-long high-finesse cavity (HFC) ($F\approx$ 200,000). The AOM, used on its order +1, interrupts the excitation once resonance with one of its longitudinal modes is achieved, leading to a ring down (RD) event. Each RD is detected with an InGaAs photodiode. The resonance is sought by adjusting the length of the cavity over $\lambda/2$ with PEEC, hosting the output mirror.

The cavity losses at each laser wavelength were obtained by averaging the results of exponential fits to some tens of ring-down events, thus giving one data point in the spectrum. The absorption coefficient, α (cm^{-1}), was then directly calculated from the decrease of the cavity ring-down time τ (in s) induced by the molecular absorption:

$$\alpha(\nu) = \frac{1}{c}\left(\frac{1}{\tau} - \frac{l}{\tau_0}\right), \quad (1)$$

where c is the light velocity and t_0 is the ring-down time of the empty cell depending of the mirror transitivity, diffraction losses, volume scattering etc…

The frequency emission of the ECDL (DL pro 1200 from Toptica) was tuned by acting on its internal grating angular position and the laser chip current, in an electronically-controlled laser-current-feed-forward scheme. The grating angular position can be roughly set with an external step motor and finely adjusted with an internal PEE_L. The ECDL has a mode-hop-free tuning range limited to 0.8 cm^{-1} obtained with a linear scan of the PEE voltage over about 80% of its full range capability. Broadband spectra were therefore obtained by concatenation of series of slightly overlapping individual narrow spectra. During automatic broadband acquisition, the laser frequency was iteratively stepped by about 0.5 cm^{-1}, by acting on the grating with the step motor. A mode-hop-free scanning situation was then automatically sought by adjusting the PEE ramp offset over successive fast (1s) test scans. The instantaneous laser frequency and the Fizeau wavemeter raw signals were used as mode hop free and monomode emission criterion, respectively. Once the optimal PEE_L

voltage offset was determined, a 10 minutes long, ~60 MHz step by step scan was started. After each frequency jump, 80 RDs were acquired before a new frequency step. In all the recordings, the sampling step was chosen to be about 2×10^{-3} cm^{-1} to be compared to a HWHM Doppler line width of about 7×10^{-3} cm^{-1} (220 MHz) and an ECDL emission linewidth of 150 kHz at 1 ms integration. Typically, the recording of a 5 cm^{-1} wide spectral interval required about one hour. Overall, the presently analysed spectrum covers the 7925-8070 cm^{-1} interval located just above the 5850-7920 cm^{-1} wide range previously studied with DFB lasers [54-64]. The most excited band of $^{16}O_3$ previously analysed is centred at 7860 cm^{-1}[63].

The absolute calibration of the frequency axis as provided by the wavemeter was refined using accurate line centres of O_2 lines that we recently reported with an accuracy better than 10^{-4} cm^{-1} [65].

B. Ozone preparation

The ozone sample was prepared using a silent electric discharge (12 kV, 400 Hz) at liquid nitrogen temperature (LNT= 77 K). This system described in Ref. [67] allows obtaining a quasi-complete conversion of oxygen to ozone after a few minutes. First, the CRDS stainless steel cell and the glass ozoniser connected with a glass tube were filled with oxygen (AlphaGaz2 from Air Liquide, purity≥ 99.9995 %) at a typical pressure of P_0= 40 Torr at room temperature. Then the ozonizer was immersed into a Dewar filled with liquid nitrogen and the discharged was switched on during a few minutes. The total pressure was observed to decrease with time during a few minutes as a result of the $3O_2 \rightarrow 2O_3$ conversion of oxygen to ozone, the latter being trapped in the ozonizer. At a residual pressure of 0.05 Torr, the discharge was interrupted and the Dewar was removed. Ozone was then evaporating leading to an initial pressure very close to $(2/3)P_0 \approx 26$ Torr of pure ozone.

The long duration required for the spectra recordings made the slow decomposition of ozone in oxygen a major issue. In order to slow down the decomposition, EPDM O-rings were used instead of Viton and their number was minimized. Vacuum grease was also avoided. The quantitative estimation of the ozone decomposition is generally obtained from the increase of the total pressure. As a result of the $2O_3 \rightarrow 3O_2$ reaction, a 1 Torr increase of the total pressure is expected to correspond to a 2 Torr decrease of the ozone partial pressure and the ozone partial pressure is deduced from the total pressure, P, measured at each spectral point $P_{O_3} = 2(P_0\text{-}P)$. The dependence of P_{O_3} *versus* the wavenumber *i.e*. *versus* time as the scanning speed of the laser frequency was constant, is presented on **Fig. 1**. During the 26 hours duration of the recordings of the displayed 7920-8012 cm^{-1} region, the ozone partial pressure is observed to decrease mostly linearly with time from 26 Torr to 17.6 Torr, with a decomposition rate of 0.2 Torr/hour. The plot includes the corresponding oxygen partial pressure obtained from $P_{O_2} = 3P\text{-}2P_0$. Interestingly, the range of the present recordings makes possible an independent determination of the oxygen partial pressure and thus to check the above pressure values. Indeed, the studied spectral interval covers part of the R branch of the $a\ ^1\Delta_g - X\ ^3\Sigma_g^-(0-0)$ band of O_2 centered at 1.27 µm. The corresponding oxygen lines can be used to determine the oxygen concentration. The resulting oxygen partial pressures deduced from the O_2 lines are plotted in **Fig. 1** together with the corresponding ozone partial pressures obtained by difference from the measured total pressure. (Note that we derived the O_2 concentration using the line intensity values recently reported in Ref. [65] which correct HITRAN values by 2-4%).

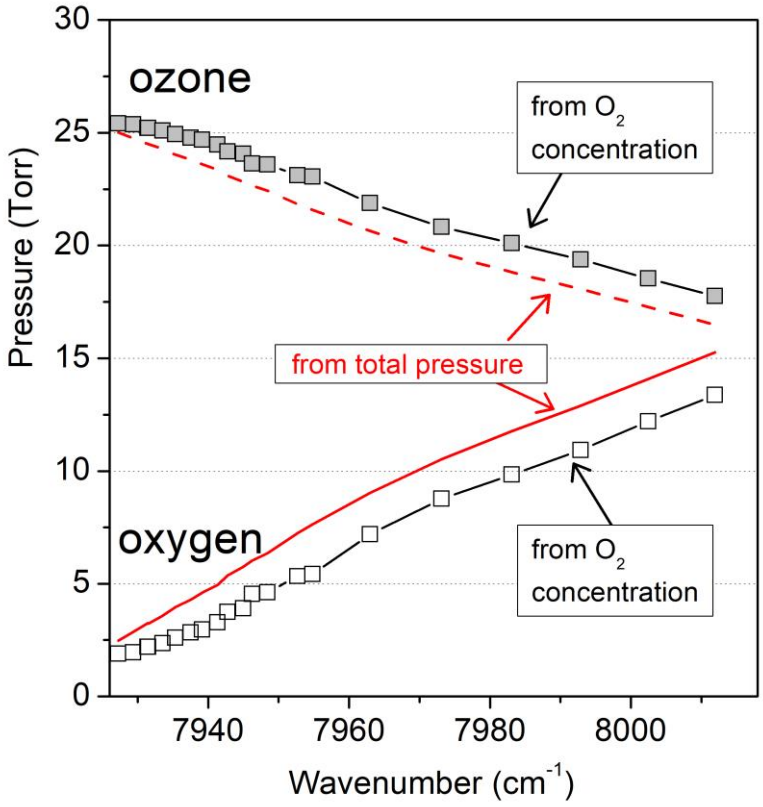

FIG. 1. Pressure variation due to the ozone decomposition in oxygen, during the CRDS recordings between 7920 and 8012 cm^{-1}. The ozone and oxygen partial pressures were determined by two independent ways: from the total pressure (dashed and solid red lines, respectively) and from the oxygen concentration derived from R branch of the $a\ ^1\Delta_g - X\ ^3\Sigma_g^-(0-0)$ band of O_2 (grey and open squares, respectively)

The two pressure determinations lead to similar wavenumber (*e.g.* time) dependences and an overall satisfactory agreement except for a mostly constant difference of about 1.2 Torr on P_{O_3}. The origin of this difference is unclear. It could be due to an incomplete ozone conversion or thermal effects. For the ozone line intensity retrieval presented below, the ozone partial pressure calculated from the total pressure was adopted. The evidenced 1.2 Torr difference between the two P_{O_3} determinations represents a fraction of P_{O_3} increasing from 4.5 to 7% over the 7920-8012 cm^{-1} region. This uncertainty on P_{O_3} is thus a major source of the overall error bar on the intensity values.

In the following, for the convenience of the data treatment, the obtained absorption coefficients were normalized to an arbitrary constant ozone pressure (*e.g.* 10. Torr).

C. Impurities and line parameters retrieval

An important difficulty of the spectrum treatment is related to the superposition of many impurity lines to the targeted ozone spectrum. In fact, as illustrated in **Fig. 2**, the spectrum is largely dominated by lines due to oxygen, water, CO_2 and HF. During the recordings, the relative concentration of these species vary according to the ozone decomposition, to desorption or chemical reaction with the walls of the setup . The strongest ozone lines observed in the region have an intensity on the order of 10^{-27} cm/molecule, which is to be compared to maximum intensity values on the order 5×10^{-26}, 5×10^{-25}, 2×10^{-26} and 3×10^{-20} cm/molecule for oxygen, water, CO_2 and HF, respectively.

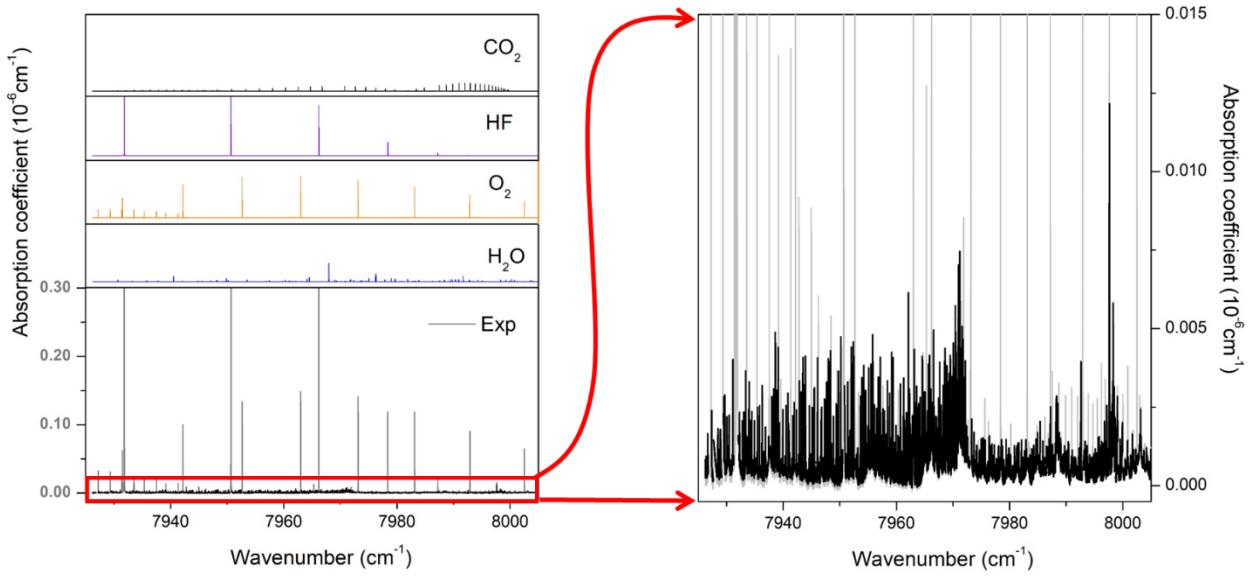

FIG. 2. Overview of the CRDS ozone recordings between 7925 and 8010 cm^{-1}. *Left panels:* Due to the weakness of the ozone spectrum, the recorded spectrum (lower panel) is dominated by impurity lines. The contributions of oxygen, water, CO_2 and HF are simulated using the HITRAN database with rough estimated relative concentration. CRDS spectrum of ozone was normalized at the ozone pressure of 10 Torr. *Right panel:* Enlargement of the ordinate scale by a factor of about 20 showing ozone bands after subtraction of the sum of the simulated contributions of the impurity species.

The relative concentrations of water, CO_2 and HF, are roughly estimated to be on the order of 10^{-3}, 2×10^{-3} and 10^{-4} for respectively while, due to ozone decomposition, oxygen partial pressure can be on the same order as the ozone partial pressure at the end of the spectra recording (see **Fig. 1**). Due to the extension and congestion of the spectrum, an accurate and systematic removal of the impurity lines from the spectrum after a careful line-by-line fit of all the absorption features was not systematically undertaken. This laborious work was limited to small spectral intervals around ozone lines which were rovibrationally assigned (see below). Nevertheless, an automatic program using as starting point a spectrum simulation using the HITRAN line lists [48] of the various impurity species with concentration dynamically adjusted according to the wavenumber, was elaborated in order to highlight the ozone contribution to the recorded spectra. The results of the procedure are presented on the right panel of **Fig. 2**. After subtraction of the impurities contribution, two ozone A-type bands showing a band head near 7973 and 7998 cm^{-1} are clearly apparent. The corresponding rovibrational assignments will be described in the following sections. It is interesting to note that the strongest absorption feature observed on the "cleaned" spectrum at about 7997.6 cm^{-1} is an ozone line belonging to the $^3A_2(0\ 0\ 0)$–$X(0\ 2\ 0)$ hot band of the Wulf electronic system. This rovibronic band center at about 8154 cm^{-1} is predissociated but show a series of narrow absorption lines which extends down to 8000 cm^{-1} and will be the subject of a separate study (see Refs. [68,69] for an analysis of a similar hot band in $^{18}O_3$).

Line parameters were determined for most of the ozone lines which could be rovibrationally assigned. The line centers and line intensities were obtained by using a homemade interactive least squares multi-lines fitting program written in LabVIEW. As the ECDL line width is much smaller than the Doppler broadening, the contribution of the apparatus function to the observed profiles was neglected. The fits were done over narrow spectral intervals including the assigned ozone lines and overlapping lines (unassigned ozone lines or impurities) which could be fitted independently. For each spectral interval, the line center, integrated absorption coefficient and Lorentzian width of each line as well as the baseline (assumed to be a linear function of the wavenumber) were provided by the fitting procedure. The Doppler broadening was fixed according to the mass of the species and the temperature of the gas. The Lorentzian width was fitted when possible or fixed to a value calculated from the default value of 0.09 cm^{-1}/atm provided by the HITRAN database for self-broadening

coefficient of ozone. Note that in our pressure conditions (about 25 Torr), the Lorentzian width (~3×10^{-3} cm^{-1} HWHM) is about half the Doppler line width (7×10^{-3} cm^{-1}).

The difficulty of the line parameter derivation due to the considerable spectral congestion is illustrated in **Fig. 3** in a spectral interval near 7948 cm^{-1}. The simulation based on the retrieved line parameters (middle panel) is compared to the experimental spectrum. The contribution of impurity lines (water and CO_2) are accounted for, and the (exp.-sim.) residuals (lower panel) correspond to a root mean square deviation of about 10^{-11} cm^{-1}. The rovibrational lines of ozone which could be assigned in the displayed region are indicated.

The line intensity, $S_{\nu_0}(T)$ of a rovibrational transition centered at ν_0, was obtained from the integrated absorption coefficient, A_{ν_0}(cm^{-2}/molecule):

$$A_{\nu_0} = \int_{line} \alpha_\nu \, d\nu = S_{\nu_0}(T)N \qquad (2)$$

Where ν is the wavenumber in cm^{-1}, α_ν is the absorption coefficient in cm^{-1} obtained from the cavity ring down time (Eq. 1) and N is the volume number density in molecule/cm^3 obtained from the measured pressure and temperature values: $P = NkT$. In the favourable cases of well isolated and relatively strong lines (we are speaking about line intensities on the order of only a few 10^{-28} cm/molecule!), the accuracy of the line positions is estimated to be about 10^{-3} cm^{-1}. Because of the moderate signal-to-noise-ratio, the statistical error of the fit leads to error bars on the integrated absorption coefficient of about 3 to 5 %. Nevertheless, taking into account frequent line overlapping and the above discussed uncertainty of the ozone partial pressure, we estimate to 10-15% the average value of the reported obtained intensity values. This is comparable or even a better precision compared to what was previously achieved in some lower wavenumber ranges for this unstable molecule.

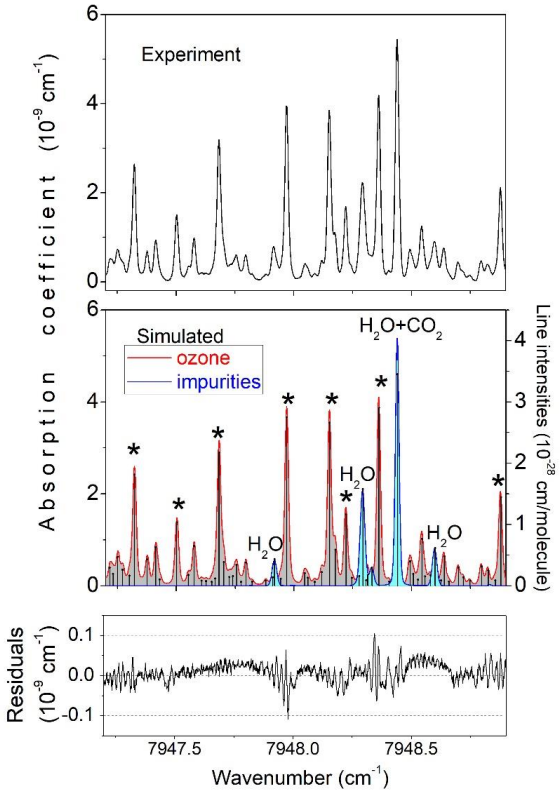

FIG. 3. Example of line parameters retrieval near 7948 cm^{-1}. *Upper panel*: CRDS spectrum normalized at the ozone pressure of 10 Torr. *Middle panel*: Absorption simulation based on the retrieved line parameters and the corresponding stick spectrum. The contribution of the ozone and impurity lines (water and CO_2) are shown in different colors (red and blue, respectively). The rovibrational lines of $^{16}O_3$ assigned in this work are marked by asterisks. *Lower panel*: (exp.-sim.) residuals. The corresponding *rms* deviation is about 10^{-11} cm^{-1}.

III. ANALYSES AND RESULTS

Two types of vibration-rotation absorption bands exist in the ozone molecule [40,42,50]. The strongest ones are activated due to the component of the dipole moment which is parallel to the a-axis of the principal inertia moment. Such bands, usually called "parallel" bands or A-type band, follow the selection rules $\Delta\upsilon_3 = odd$ and $\Delta K_a = even$. The second type of bands are the "perpendicular" bands or B-type bands which follow the selection rules $\Delta\upsilon_3 = even$ and $\Delta K_a = odd$. Within the same frequency interval, these latter bands are usually weaker and have quite irregular line intensity patterns making more difficult their rovibrational assignment. Due to their weakness and irregular structure, perpendicular bands have not been assigned in wavenumber ranges above 6770 cm^{-1} [42,63]. However, the corresponding upper states play the role of "dark" states which may perturb observed "bright" states *via* accidental resonance interactions [42].

Many previous studies have made it clear that vibrational extrapolation using standard Dunham-type expansion [70] in terms of quantum numbers $\upsilon_1,\upsilon_2,\upsilon_3$ does not give reliable results for the ozone band centres near the dissociation threshold. In this work, the identification of new bands in the recorded CRDS spectrum relied on the variational predictions from the *ab initio* PES reported in Ref. [26] where the "global" vibrational assignment (Γ, N) was given by the irreducible representation Γ of C_{2V} point group and the ranking number N, increasing with energy.

In the 7920-8000 cm^{-1} range of the present recordings, eight vibrational levels of A_1 and B_1 types in C_{2V} point group are predicted [26]. Four of them - (B_1, N=87-90) at 7928.76, 7944.73, 7971.69 and 7991.66 cm^{-1}, respectively, - belong to the B_1 irreducible representation (anti-symmetric with respect to the C_2 axis). Note that for B_1 vibrational levels, J= 0 states are not spin-allowed [40, 42] because all ^{16}O nuclei of the main ozone isotopologue, $^{16}O_3$, are bosons. However, the calculation of such states, *via* the diagonalization of *ab initio* based vibrational Hamiltonian, is meaningful because they correspond to observable band centres obtained as $J\rightarrow 0$ limit of experimental rotational line series. The $J > 0$ rovibrational states of B_1 vibrational levels do exist, and the transitions to these states correspond to parallel ($A_1^{vib}\rightarrow B_1^{vib}$) bands, which are determined experimentally. Another four vibration levels belonging to totally symmetric A_1 irreducible representation are predicted: (A_1, N=117-120) at 7943.77, 7949.65, 7957.13 and 7973.76 cm^{-1}, respectively. They could give rise to very weak perpendicular ($A_1^{vib}\rightarrow A_1^{vib}$) bands with hardly assignable tiny and irregular patterns, which do not exhibit characteristic band heads [add refs].

As in previous studies [52, 71], to help the assignment, the rovibrational J= 1 and J= 2 levels were computed from the *ab initio* PES [26] and used to determine theoretical values of A_V, B_V and C_V rotational constants of the different predicted vibrational states. Their comparison with observations will be discussed in section IV.

A. Spectra assignment

The effective Hamiltonian (EH) and effective dipole moment (EDM) models were used for the assignments. The basic definitions and technical details can be found in Refs. [39,40,42,50]. The iterative fits of observed transitions and elaboration of calculated line lists used the GIP program [72]. At the initial iteration, *ab initio* values [26] were adopted for the band centers and rotational constants involved in the EH model as the adjustable parameters. This allows us for following series of lines with increasing total rotational quantum number J for various values of K_a. In general, the (ν_{obs}-ν_{calc}) position difference *versus* rotational quantum numbers showed a smooth dependence until a resonance perturbation appears. A comparison of the corresponding deviation curves as a function of K_a permits assigning few lines for low values of rotational quantum numbers. A second way, particularly relevant for A-type bands in the CRDS spectral range, was to look at the sharp observed band head in the R-branch, trying various assignments and seeking the same (ν_{obs}-ν_{calc}) residuals in the P-branch. Successive fits of EH parameters allowed us to assign more and more lines by iterations.

The most complicated issue was the modeling of irregular deviations from a single-vibration-state model, which appears to be due to perturbations caused by resonance interactions with "dark" states. This problem becomes very difficult to solve at high energy range where the density of rovibrational states drastically increases towards the dissociation threshold. In these conditions, EH models suffer from lack of experimental information for numerous closely lying "perturber states". For this reason the *rms* (ν_{obs}-ν_{calc}) deviations of the EH fits systematically increase with vibration energies (see Fig. 7 of Ref. [26]). Another difficulty is that many observed lines are blended or hidden by impurities or unidentified ozone lines, including hot band vibronic transitions. To overcome the shortcomings of incomplete EH models, we have determined effective parameters specific for different J, K_a series by separating the data according to the parity of J for K_a = 1, 2 and 3. This permitted extending assignments with smaller partial *rms* deviations for separate series of lines.

As far as possible, ground state combination differences (GSCD) relations from transitions belonging to *P*-, *R*- or *Q*-branches, were checked to insure the assignments. In addition, we also verified that relative intensities calculated with an approximate value of the fitted effective dipole moment were qualitatively consistent with the observations, thanks to synthetic spectra computed by MULTIFIT program [73].

1. The $\nu_1+6\nu_2+3\nu_3$ band in the 7930-7973 cm^{-1} range

The position of the band head observed at 7973 cm^{-1} (see **Fig. 2**) points the (B_1, N=89) upper state at 7971.69 cm^{-1} as most probable candidate for the upper state of the corresponding parallel band. This is consistent with simulations using t*ab initio* values of the corresponding rotational constants which indicate that the centre of the observed band should lie about 2-3 cm^{-1} below the sharp absorption feature of the band head. The (B_1, 89) upper vibration level is assigned as (υ_1,υ_2,υ_3) = (1,6,3). This vibrational assignment relies on the decomposition of the corresponding *ab initio* wavefunction in the normal mode basis set using the contact transformation (CT) method. To this end, we used MOL_CT program suite [74,75]; the technical aspects of calculations were described in [71,74,75].

(a) Line positions and energy levels. The first series of assignments concerned the K_a = 4 upper state levels abd was validated by GSCD relations involving the *P*-, *Q*- and *R*-branches. Then, a similar procedure was applied to other K_a values leading to the assignment of 243 transitions of the $\nu_1+6\nu_2+3\nu_3$ band reaching a total of 130 upper state energy levels. The experimentally determined energy levels are listed in **Table I** with their corresponding statistical error bars when they could be derived from different transitions.

A fit of the experimental line positions using an isolated state EH model leads to an *rms* deviation of 0.148 cm^{-1}, largely above the experimental uncertainty. Deviations between measured and calculated position values were found to be either positive or negative, depending on the parity of J, without smooth dependence on rotational quantum numbers. Particular large perturbations were detected for K_a = 1 and 2 series. The introduction of a Coriolis interaction with the (A_1,118) dark state predicted at 7949.65 cm^{-1} [26] allowed for a reduction of the *rms* deviation by a factor of two (0.078 cm^{-1}). The set of derived parameters is given in **Table II**. Note that the mixing coefficient between J, K_a, K_c =14, 2, 13 state of the (B_1, 89) state and J, K_a, K_c =14, 3, 11 of the (A_1,118) state is about 50-50 % making an assignment of this particular rovibrational level ambiguous.

Table I. Rovibrational energy levels derived from observed transitions for the (1,6,3) and (6,1,1) vibration states of $^{16}O_3$.

									continued								
$(\upsilon_1,\upsilon_2,\upsilon_3)$:			**(1,6,3)**			**(6,1,1)**						**(1,6,3)**			**(6,1,1)**		
J	K_a	K_c	*E* (cm^{-1})	*Nb*	Δ*E*	*E* (cm^{-1})	*Nb*	Δ*E*	*J*	K_a	K_c	*E* (cm^{-1})	*Nb*	Δ*E*	*E* (cm^{-1})	*Nb*	Δ*E*
1	0	1	7969.5294	1		7993.6164	1		13	2	11	8049.7297	2	0.1	8077.0688	1	
1	1	0				7996.6583	2	0.0	13	3	10	8064.2333	2	0.2	8091.8783	2	0.8
2	1	2	7974.0368	1		7998.1394	2	1.2	13	4	9	8085.6814	3	0.3	8112.4860	1	
2	2	1	7983.3140	1		8007.2677	1		13	5	8	8113.2495	3	0.2	8139.6000	2	0.9
3	0	3	7973.2411	1		7997.5429	2	0.7	13	6	7	8146.9147	2	0.7	8172.5748	2	0.5
3	1	2				8000.7153	1		13	7	6	8186.7142	2	0.1			
3	2	1	7985.5595	2	0.3	8009.6269	2	0.1	14	1	14	8046.6396	2	0.2	8075.5942	1	
3	3	0	8000.9057	1		8024.7016	2	0.2	14	2	13				8087.2677	2	0.2
4	1	4	7979.1191	2	0.1	8003.4646	1		14	3	12	8074.6230	1		8102.8590	1	
4	2	3	7988.5467	1		8012.7694	3	0.3	14	4	11	8096.1139	2	0.2	8123.4674	2	0.6
4	3	2	8003.8791	3	0.3	8027.7930	1		14	5	10	8123.6803	3	0.7	8150.5991	2	0.1
4	4	1	8025.3594	1		8048.9209	1		14	6	9	8157.3485	2	0.5	8183.5544	2	0.5
5	0	5	7979.9085	2	0.0	8004.6010	2	0.6	14	7	8	8197.1597	2	0.1			
5	1	4	7983.4015	2	0.1	8008.0042	1		15	0	15	8056.4647	2	0.0	8085.8301	2	0.2
5	2	3	7992.3147	2	0.3	8016.7197	3	0.5	15	1	14	8063.7405	2	0.0	8092.6683	2	0.4
5	3	2	8007.5955	1		8031.6599	2	0.1	15	2	13	8071.8674	2	0.1	8100.2682	1	
5	4	1	8029.0788	1		8052.8445	2	0.2	15	3	12	8085.9023	2	0.1	8114.7291	1	
5	5	0	8056.6525	2	0.4	8079.8977	1		15	4	11	8107.3017	3	1.0	8135.2315	1	
6	1	6	7987.1440	2	0.6	8011.8310	2	0.5	15	5	10	8134.8562	3	1.5	8162.3864	2	0.8
6	2	5	7996.7518	3	0.1	8021.4119	2	1.0	15	6	9	8168.5267	2	0.7	8195.2969	3	0.9
6	3	4	8012.0628	1		8036.2627	1		15	7	8	8208.3566	2	0.6			
6	4	3	8033.5441	3	0.7	8057.5532	2	0.5	16	1	16	8069.2015	2	0.2	8099.0372	1	
6	5	2	8061.1204	2	0.2	8084.6104	1		16	2	15				8111.5025	2	0.6
6	6	1	8094.7657	1		8117.5858	1		16	3	14	8097.7524	2	0.6	8127.2479	2	0.0
7	0	7	7989.5056	1		8014.7591	1		16	4	13	8119.2302	2	0.0			
7	1	6	7993.3939	2	0.2	8018.5229	2	0.1	16	5	12	8146.7797	3	0.8	8174.9631	2	0.1
7	2	5	8002.0477	2	0.6	8026.9860	2	0.5	16	6	11	8180.4505	2	0.9			
7	3	4	8017.2666	2	0.4				16	7	10	8220.3162	2	1.6			
7	4	3	8038.7549	2	0.0	8063.0481	2	0.1	17	0	17	8080.2014	2	0.0	8111.0405	1	
7	5	2	8066.3336	1		8090.1066	3	0.2	17	1	16	8088.8058	2	0.2	8119.1313	1	
7	6	1	8099.9823	2	0.3	8123.0871	1		17	2	15	8097.1639	2	0.5	8126.7428	1	
7	7	0	8139.7261	1					17	3	14	8110.6071	2	0.3	8140.7770	2	0.3
8	1	8	7997.8048	1		8023.2820	2	0.0	17	4	3	8131.9187	1				
8	2	7	8007.9584	1		8033.1941	2	0.4	17	5	12	8159.4508	2	0.2	8188.3177	1	
8	3	6	8023.1759	2	0.1	8048.6488	1		17	6	1	8193.1237	2	0.4			
8	4	5	8044.7091	1		8069.3261	3	0.3	17	7	0	8232.9711	1				
8	5	4	8072.2890	2	0.3	8096.3904	2	0.3	18	1	18	8093.4451	1		8125.4869	1	
8	6	3	8105.9426	2	0.2	8129.3746	2	0.8	18	2	17				8138.8183	1	
8	7	2	8145.6921	3	0.7				18	3	16	8123.8834	2	0.4	8154.7910	1	
9	0	9	8001.9979	1		8027.9996	2	0.3	18	4	15	8145.3442	2	0.6			
9	1	8	8006.4413	2	0.3	8032.2651	2	0.4	18	5	14	8172.8712	1		8202.4610	2	0.5
9	2	7	8014.8527	2	0.4	8040.4497	1		18	6	13	8206.5448	2	0.4			
9	3	6	8029.9235	2	0.4	8055.7098	3	0.6	18	7	12	8246.4216	1				
9	4	5	8051.4112	2	0.4	8076.3875	2	0.0	19	0	19	8106.7415	2	0.5	8139.1848	1	
9	5	4	8078.9957	1		8103.4616	3	0.4	19	1	18	8116.7904	1				
9	6	3	8112.6463	2	0.5	8136.4454	3	0.5	19	2	17	8125.6173	2	0.0	8156.4829	1	
9	7	2	8152.4021	3	0.4				19	3	16	8138.3634	2	0.1	8170.0370	1	
10	1	10	8010.7210	1		8037.6875	2	0.7	19	4	15	8159.5516	1				
10	2	9	8022.1628	2	0.0	8048.1028	2	0.7	19	5	14	8187.0380	2	0.4	8217.3867	1	
10	3	8	8037.3507	2	0.1	8063.5567	2	0.5	19	6	13	8220.7143	2	0.1			
10	4	7	8058.8605	1		8084.2362	2	0.3	20	1	20	8121.3250	1				
10	5	6	8086.4358	3	0.1	8111.3170	3	0.2	20	2	19				8169.1989	2	0.5
10	6	5	8120.0957	2	0.7	8144.3052	1		20	3	18	8153.0237	2	0.1	8185.4851	1	
10	7	4	8159.8598	2	0.0				20	4	17	8174.4616	2	0.0			
11	0	11	8017.3447	2	0.2	8044.2821	2	0.4	20	5	16	8201.9579	2	0.5	8233.0670	1	
11	1	10	8022.5294	2	0.2	8049.2157	2	0.3	20	6	15	8235.6359	2	0.1			
11	2	9	8030.7350	2	0.4	8057.1341	2	1.1	20	7	14	8275.5665	2	0.5			
11	3	8	8045.5758	2	0.2	8072.2030	1		21	0	21	8136.3201	2	0.3	8170.2547	2	0.2
11	4	7	8067.0537	2	0.5	8092.8695	3	0.7	21	1	20	8147.6594	2	0.3			
11	5	6	8094.6283	3	0.3	8119.9577	3	0.3	21	2	19	8157.2112	2	0.0			
11	6	5	8128.2870	1		8152.9438	2	0.0	21	3	18	8169.1961	2	0.4	8202.5291	1	
11	7	4	8168.0643	1					21	5	16	8217.6239	3	1.2			
12	1	12	8027.2777	2	0.0	8055.1341	1		21	6	15	8251.3031	1				
12	2	11	8039.4034	2	0.0	8066.1303	2	0.2	22	2	21				8202.6317	2	1.3
12	3	10	8054.4907	2	0.4	8081.6279	2	0.0	22	3	20	8185.1884	2	0.2	8219.3199	2	0.2
12	4	9	8075.9933	3	0.2	8102.2870	2	0.7	22	5	18	8233.9755	1				
12	5	8	8103.5671	3	0.9	8129.3868	3	0.2	23	0	23				8204.2476	2	0.5
12	6	7	8137.2301	3	0.6	8162.3699	1		23	3	20				8238.2803	1	
12	7	6	8177.0147	2	0.9				24	3	22				8256.2835	1	
13	0	13	8035.5106	2	0.3	8063.5688	2	0.3	25	3	22				8277.2962	2	0.7
13	1	12	8041.6376	2	0.0	8069.3585	2	0.4									

Notes: Nb is the number of observed transitions used to determine the upper energy level *E* (cm^{-1}). Δ*E* is the *rms* error of the experimental energy determination (in 10^{-3} cm^{-1} unit).

Table II. Spectroscopic parameters and fit statistics for the $\nu_1+6\nu_2+3\nu_3$ band of $^{16}O_3$ band centred at 7968.8 cm^{-1}.

(i) Spectroscopic parameters (cm^{-1})					*(iii)* Statistics for line positions	
Upper states		(1,6,3) ≡ (B_1,89)	(A_1,118) dark state		J_{max}	22
E^{VV}		7968.782_6 (18)	7949.76_1 (34)		$K_{a\ max}$	7
A-(B+C)/2		3.0769_8 (15)	3.164_6 (33)		Number of transitions	243
(B+C)/2		0.37138_7 (18)	0.38564_4 (95)		Number of levels	130
(B-C)/2		0.03044_4 (45)	0.0255 [f]		*rms* (cm^{-1}) [a]	0.078
Δ_K	$\times10^3$	0.300_9 (30)			*(iv)* Statistics for line intensities	
Δ_{JK}	$\times10^4$	-0.229_6 (39)			*J* max	22
Δ_J	$\times10^5$	-0.152_3 (71)			K_a max	7
δ_J	$\times10^5$	0.603_6 (52)			Number of transitions	182
δ_K	$\times10^3$	-0.203_3 (91)			*rms* (%)[a]	12.0
Coriolis coupling between (A_1,118) and (1,6,3) states					S_v = 4.18×10^{-26} cm/molecule at 296 K[b]	
C_{011}		0.0172_5 (16)				
(ii) Dipole transition moment parameters (Debye)						
$d_1^{(A)}$	$\times10^5$	0.6028_4 (62)	$d_4^{(A)}$ $\times10^7$	-0.118_9 (16)		
$d_2^{(A)}$	$\times10^8$	-0.1568_4 (81)	$d_6^{(A)}$ $\times10^7$	0.390_3 (50)		
$d_3^{(A)}$	$\times10^8$	-0.397_4 (83)				

Notes

[a] Two transitions to the upper state level *J*, K_a, K_c =21, 2, 19 were excluded from the fit.

[b] Sum of intensities in the combined line list (366 lines).

[f] - fixed to the values predicted from the PES of Ref. [26]. All higher order centrifugal distortion parameters [77] quoted in [78] were held fixed to their ground state values. Grey background corresponds to the ($\Gamma=A_1$, N=118) dark state.

(b) Line intensities and effective dipole transition moment. The empirical determination of weak band transition moments from crowded spectra is quite sensitive to uncertainties of experimental intensities and to the completeness of underlying theoretical model. Among the assigned transitions of the $\nu_1+6\nu_2+3\nu_3$ band, a subset of 182 relatively isolated lines sampling the *P*-, *Q*- and *R*-branches was selected. Depending on the proximity with other lines, realistic error bars were evaluated and associated to the corresponding line intensities. The intensity values were used as input data of a weighted fit of the EDM parameters. The standard EDM model [79,80] for A-type bands of C_{2V} molecules were adopted [79,80]:

$$
\begin{aligned}
{}^{(V^u)(V^l)}\tilde{\mu}_Z^{(A)} = d_1^A\varphi_z + d_2^A\left\{\varphi_z,\mathbf{J}^2\right\} + d_3^A\left\{\varphi_z,J_z^2\right\} + d_4^A\frac{1}{2}\left[\left\{\varphi_x,iJ_y\right\} - \left\{i\varphi_y,J_x\right\}\right] + \\
d_5^A\frac{1}{2}\left[\left\{\varphi_x,J_xJ_z+J_zJ_x\right\} - \left\{i\varphi_y,\mathrm{i}(J_yJ_z+J_zJ_y\right\}\right] + d_6^A\frac{1}{2}\left[\left\{\varphi_x,iJ_y\right\} + \left\{i\varphi_y,J_x\right\}\right] + \ldots\ ,
\end{aligned}
\tag{3}
$$

where the notation $\{\mathrm{X},\mathrm{Y}\} = XY + YX$ stands for an anti-commutator, φ_α are direction cosines for the Eckart molecular fixed frame, J_α are the molecular fixed component of the total angular momentum, and $d_i^{(A)}$ are band-specific transition moment parameters empirically retrieved from the line intensities of the observed band. Five parameters of the effective dipole transition moment could be well determined with a weighted standard deviation 1.061 and an *rms* deviation of 12 %. The results of the fit are provided as a Supplementary Material while the derived EDM parameters are listed in **Table II** together with corresponding fit statistics. The comparison of the measured and calculated line intensities for the 182 lines included in the fit is presented in **Fig. 4**.

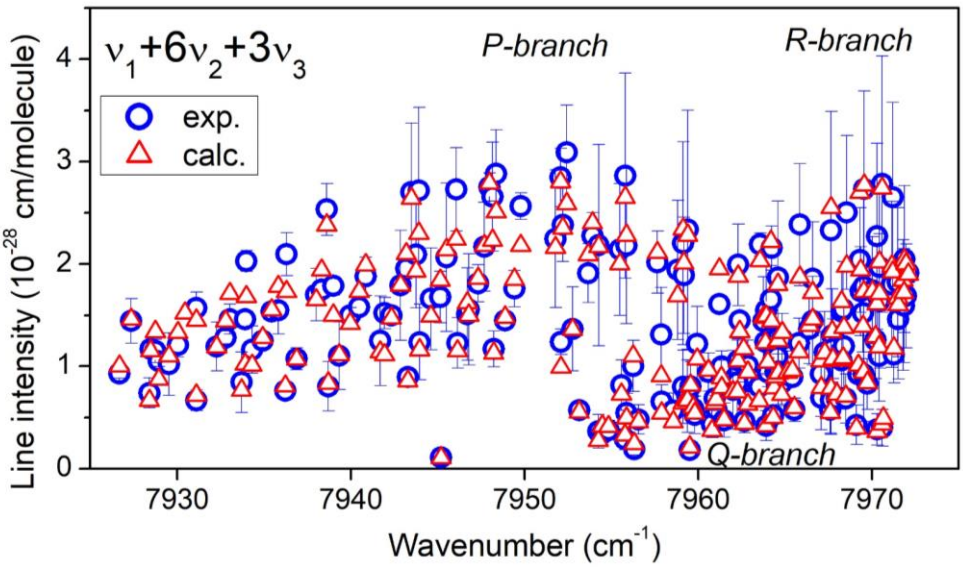

FIG. 4. Comparison for the measured and calculated line intensities for the selected set of 182 lines used to fit of effective dipole moment of the $\nu_1+6\nu_2+3\nu_3$ band. Error bars correspond to estimated experimental uncertainties.

(c) Line list and comparison with observations.

A list of 366 transitions of the $\nu_1+6\nu_2+3\nu_3$ band allowed by $\Delta K_a = 0$ selection rule was generated using the EH and EDM parameters of **Table II**. The list was limited to transitions reaching experimentally determined upper state levels and line positions were empirically corrected according to the experimental value of the upper energy levels listed in **Table I**. Line intensities were computed using the fitted EDM parameters and wavefunctions corresponding to the EH of **Table I**. Note that the resulting list includes a number of lines unobserved in the spectrum (*e.g.* hidden by impurity lines) which have experimental accuracy on their line centers because they reach an upper level empirically determined from different transitions. The obtained line list leads to the overview comparison presented in **Fig. 5.**

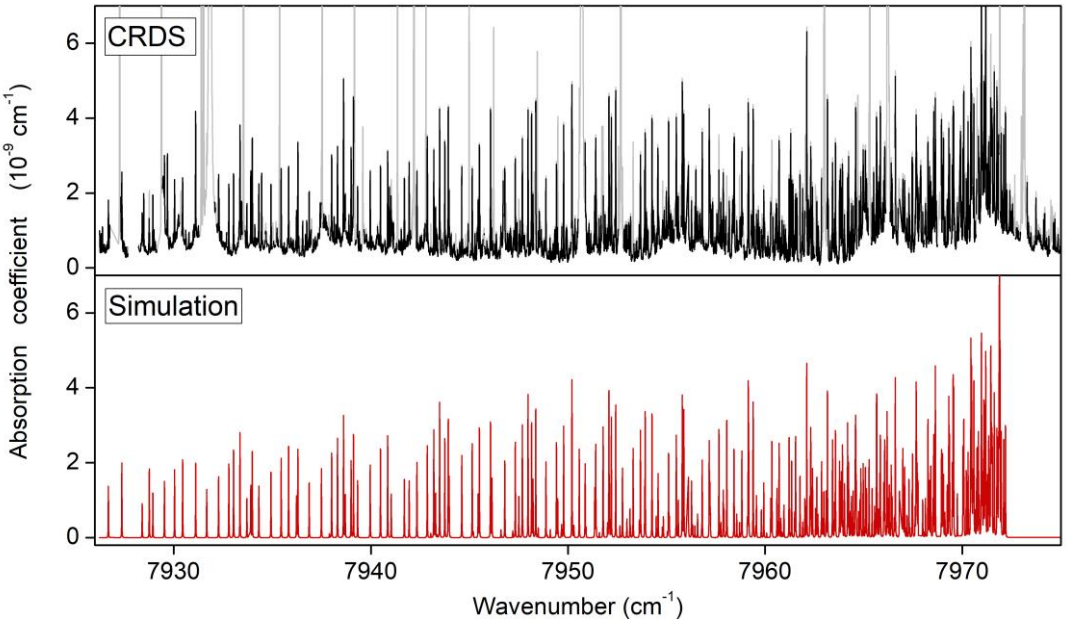

FIG. 5. Overview of the $\nu_1+6\nu_2+3\nu_3$ absorption band of $^{16}O_3$. *Upper panel*: CRDS spectrum with impurity lines (partly) removed at a pressure normalized to 10 Torr (the grey trace corresponds to the original CRDS spectrum with impurity lines). *Lower panel*: simulation limited to transitions reaching experimentally determined upper levels with intensities computed from EH and EDM (**Table II)** and line positions empirically corrected.

More detailed blown-up comparisons in the *P* and *R*-branches are shown in **Figs. 6** and **7.** These figures provide extended qualitative validation of the assignments and of intensities computed from the fitted effective dipole transition moments of **Table II**. They contain supplementary information with respect to **Fig. 4** concerning absorption features composed of doublet, triplet and other overlapping lines, which were not possible to include in the dipole moment fit. The account for new computed transitions (beyond 182 intensities included in the fit - **Fig. 4**) are particularly important for the *R*-branch (**Fig. 7**) because they contribute to overlapping lines near the compressed band head, which correspond to the strongest absorption features of the band.

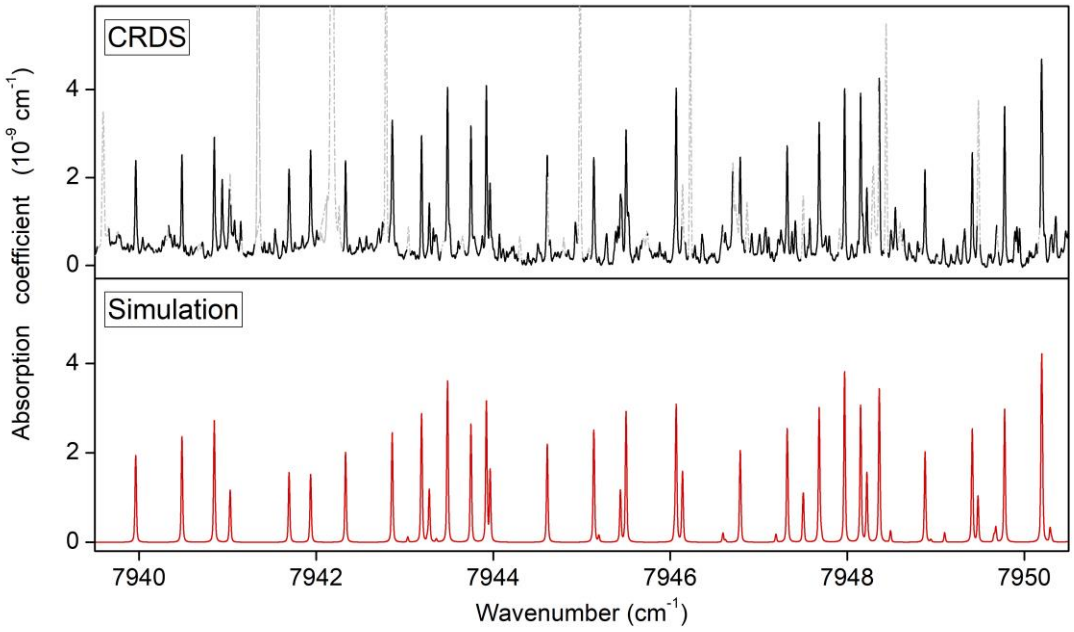

FIG. 6. Example of comparison of CRDS and simulated spectra in the *P*-branch region in the $\nu_1+6\nu_2+3\nu_3$ band. *Upper panel*: CRDS spectrum with impurity lines (partly) removed (black). The original spectrum including impurity lines is also displayed (dashed grey) *Lower panel*: simulation limited to transitions reaching experimentally determined upper levels with intensities computed from EH and EDM (**Table II**) and line positions empirically corrected.

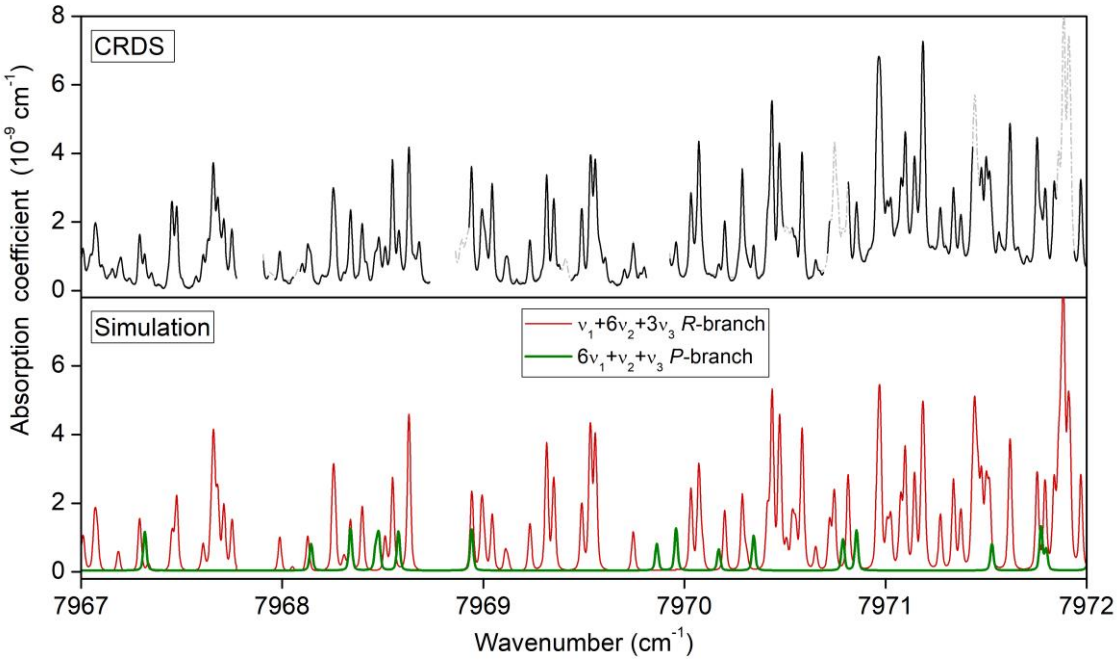

FIG. 7. Same as Fig. 6 in the *R*-branch region of the $\nu_1+6\nu_2+3\nu_3$ band. A few lines (green) correspond to a simulation of the *P*-branch of the $6\nu_1+\nu_2+\nu_3$ band (see next Section A.2).

2. The $6\nu_1+\nu_2+\nu_3$ band in the range 7951-8000 cm^{-1}

A head of a weak vibration-rotation band is observed near 7998 cm^{-1}, (**Fig. 2**) but it is superimposed with H_2O impurity lines, other ozone lines in particular some strong absorption features due to vibronic transitions of the $^3A_2(0\ 0\ 0)$–$X(0\ 2\ 0)$ hot band of the Wulf electronic, making the assignment more challenging. According to the *ab initio* predictions, the (B_1, 90) vibrational level predicted at 7991.66 cm^{-1} [26] is the most plausible candidate for the upper state of this A-type band. This is confirmed by calculations using the theoretical values of rotational constants which predict a band head agreeing with the observations within about 1 cm^{-1}. The decomposition of the (B_1,90) *ab initio* wavefunction in the normal mode basis gives a major contribution to the (υ_1,υ_2,υ_3) = (6,1,1) normal mode vibration. Consequently, the corresponding parallel absorption band was assigned as $6\nu_1+\nu_2+\nu_3$. Note that the low energy neighbor of the (B_1, 90) level -(B_1, 89)- is the upper level of the $\nu_1+6\nu_2+3\nu_3$ parallel band assigned above, whereas the next parallel band (B_1, 91) is predicted 52 cm^{-1} [26] above the observed band head.

(a) Line positions and energy levels. Following the above described techniques, 189 transitions of the $6\nu_1+\nu_2+\nu_3$ band corresponding to 110 upper state energy levels could be assigned. It appeared that the $K_a = 3$ series was strongly perturbed. Thanks to *ab initio* predictions [26], this perturbation was identified as a strong Coriolis resonance with the $K_a = 4$ levels of the (A_1,119) vibrational state predicted at 7957.13 cm^{-1} and confirmed by next assignments. The introduction of this dark state in the EH model permitted reducing the final *rms* deviation in line positions from 0.12 to 0.016 cm^{-1}. The fitted values of the spectroscopic parameters are given in **Table III**. The experimentally determined values of the (611) rovibrational levels are included in **Table I.**

Table III. Spectroscopic parameters and fit statistics for the $6\nu_1+\nu_2+\nu_3$ band of $^{16}O_3$centred at 7992.6 cm^{-1}.

(i) Spectroscopic parameters (cm^{-1})			*(iii)* Statistics for line positions	
Upper states	(A1,119) state	(611)	J_{max}	25
E^{VV}	7962.623_5 (56)	7992.8307_5 (35)	$K_{a\ max}$	6
A-(B+C)/2	3.6674 [f]	3.02065_4 (42)	Number of transitions	189
(B+C)/2	0.37059_9 (77)	0.392989_5 (31)	Number of levels	110
(B-C)/2	0.0263 [f]	0.024256_9 (24)	*rms* (cm^{-1})	0.016
Δ_K $\times10^3$		0.400_3 (12)	*(iv)* Statistics for line intensities	
Δ_{JK} $\times10^5$		-0.32_7 (15)	*J* max	18
Δ_J $\times10^6$		0.827_7 (50)	K_a max	6
Coriolis coupling term between (611) and (A1,119) (cm^{-1}):			Number of transitions	67
C_{011}	-0.01954_5 (24)		*rms* (%)	15.5
(ii) Dipole transition moment (Debye)			$S_v = 1.36\times10^{-26}$ cm/molecule at 296 K [a]	
$d_1^{(A)}$ $\times10^5$	0.3187_0 (26)			

Notes

[a] Sum of intensities in the combined list (306 lines).

[f] - fixed to the values predicted from the PES of Ref. [26]. All higher order centrifugal distortion parameters [77] quoted in [78] were held fixed to their ground state values. Grey background corresponds to the ($\Gamma=A_1$, N= 119) dark state.

(b) Line intensities and effective dipole transition moment. As for the previous band, a restricted set of relatively isolated lines were used for the determination of the EDM parameters. Note that the weakness of the band (line intensities between 10^{-29} and 10^{-28} cm/molecule) results in larger uncertainties on the intensity values. Only the principal transition moment parameter could be determined from the weighted fit of 67 line intensities belonging to *P*-, *Q*- and *R*-branches (weighted standard deviation of 1.009 and the *rms* deviation of 15.5% - see **Table III** and Supplementary Materials). The general agreement between the measured and fitted intensity values is illustrated in **Fig. 8**.

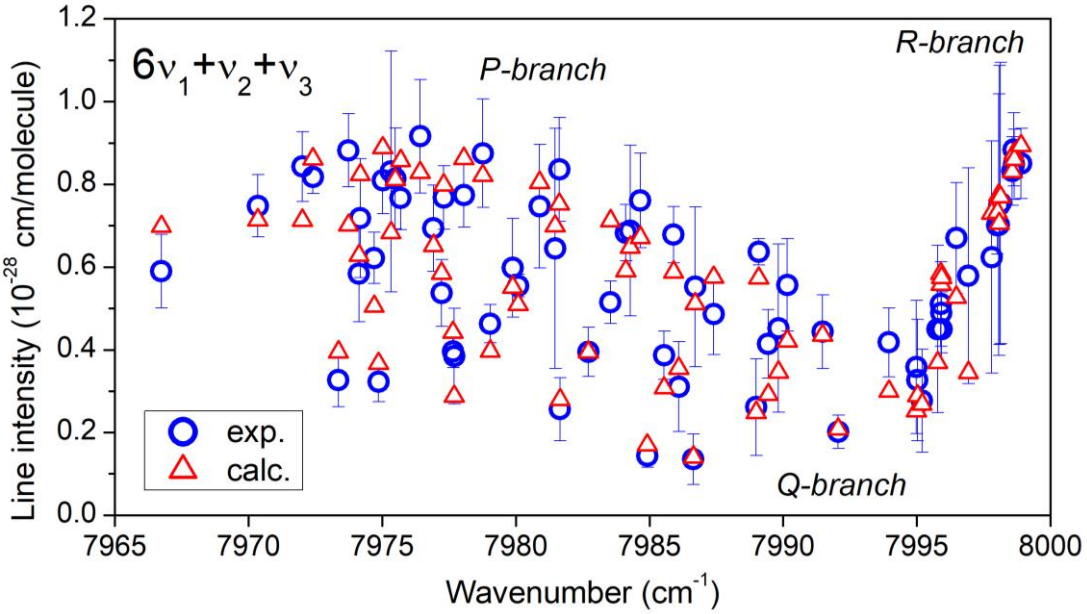

FIG. 8. Comparison for the measured and calculated intensities for the selected set of 67 lines band used to fit of effective dipole moment of the $6\nu_1+\nu_2+\nu_3$ band. Error bars correspond to estimated experimental uncertainties.

(c) Line list and comparison with observations. In the same way as for the $\nu_1+6\nu_2+3\nu_3$ band, a line list reaching the experimentally determined energy level of the (611) state was generated. Line positions were adjusted according to the experimental energy values (**Table I**) while line intensities were computed using the EDM parameters and EH eigenfunctions (**Table III**). The list provided as Supplementary Material includes 306 transitions up to J_{max} = 25, $K_{a\ max}$ = 6. The sum of their calculated intensities is $S_V = 1.3\times10^{-26}$ cm/molecule, a factor of three smaller than for the $\nu_1+6\nu_2+3\nu_3$ band.

Fig. 9 and **10** show an overview comparison of the simulated absorption coefficient using this combined line list of the $6\nu_1+\nu_2+\nu_3$ band (lower panel) to the CRDS spectrum (upper panel) in the *P*- and *R*-branch region, respectively. Let us note that the CRDS spectrum is formed by narrow rovibrational lines superposed to broad diffuse structures. Based on the previous works of Bouvier et al. and Abel et al.[add refs!] on the $^3A_2$(0 0 0)–X(0 0 0) rovibronic band of $^{16}O_3$ near 10080 cm^{-1} and on previous observations of similar broad structures assigned to the $^3A_2$(0 0 0)–X(1 1 0) hot band of the heavy $^{18}O_3$ isotopologue near 7880 cm^{-1} band [16,17], these diffuse absorption patterns are believed to be due to rovibronic transitions reaching the metastable levels of excited electronic $^3A_2$ triplet state from the (0 2 0) bending state at 1399 cm^{-1} (the center of the $^3A_2$(0 0 0)–X(0 2 0) hot band is predicted near 8154 cm^{-1}). In addition, to these rovibronic structures (two narrow ones are marked on **Fig. 10**), the very weak lines of the $6\nu_1+\nu_2+\nu_3$ band are superimposed to strong lines of impurities (in particular water and CO_2) and other narrow lines which are believed to belong to ozone but remain to be identified. To make the comparison clearer, we have extracted in the middle panel of **Fig. 9**, the lines of the $6\nu_1+\nu_2+\nu_3$ band for which line parameters were derived from a fit of their line profile. A care has to be taken for interpretation of fine details in such comparison because of the presence of overlapping multiplets, some of them not belonging to the assigned band. However, the general agreement of the intensity patterns in the measured (middle panel) and calculated (lower panel) spectra validates the assignments of the $6\nu_1+\nu_2+\nu_3$ band.

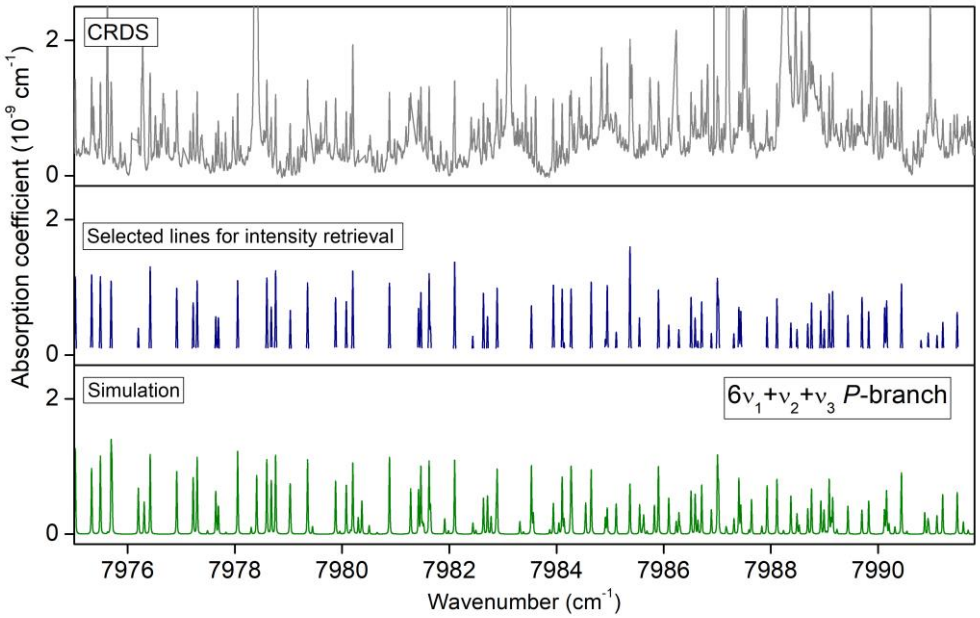

FIG. 9. Spectrum overview in the region of *P*-branch of the $6\nu_1+\nu_2+\nu_3$ band of $^{16}O_3$. *Upper panel*: CRDS spectrum including the $6\nu_1+\nu_2+\nu_3$ band, impurity lines (water and CO_2), broad structures due to the $^3A_2(0\ 0\ 0)$–$X(0\ 2\ 0)$ hot band of $^{16}O_3$ and additional unidentified lines of ozone. *Middle panel*: lines of the $6\nu_1+\nu_2+\nu_3$ band of $^{16}O_3$ which were reproduced with a Voigt profile fit. The plotted lines are simulations based on the retrieved line profile parameters *Lower panel*: simulation limited to transitions reaching experimentally determined upper levels with intensities computed from EH and EDM (Table I) and line positions empirically corrected.

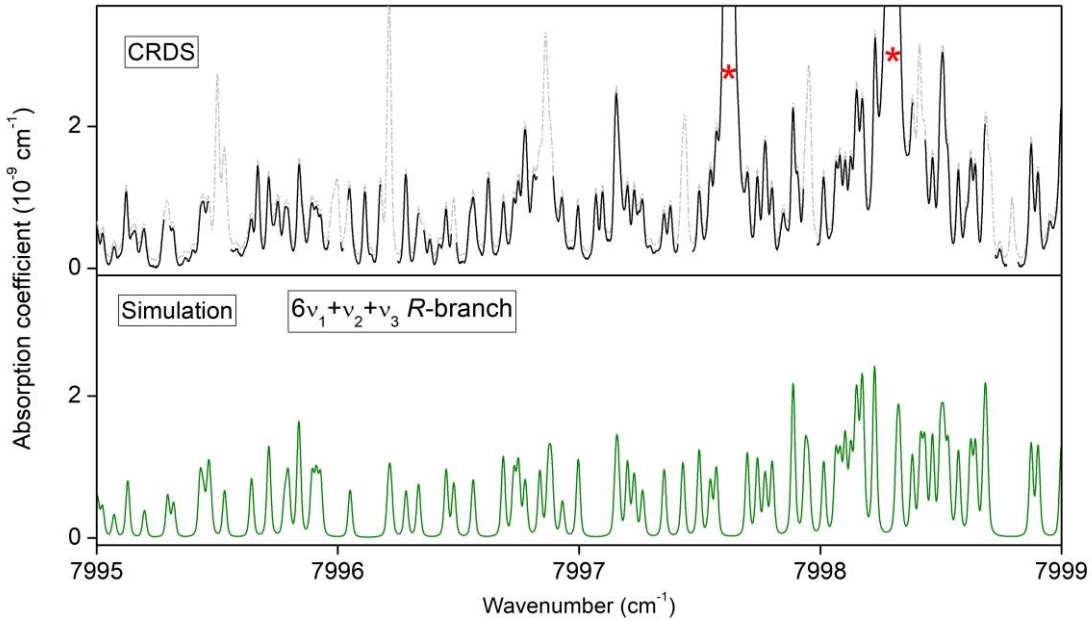

FIG. 10. Same as Fig. 9 in the region *R* branch of the $6\nu_1+\nu_2+\nu_3$ band of $^{16}O_3$. The original spectrum including impurity lines is also displayed on the upper panel (dashed grey) Relatively broad features marked with asterisks correspond to electronic $^3A_2(0\ 0\ 0)$ - $X\ ^1A_1(020)$ hot band transitions

In order to illustrate the difficulty of the analysis of the $6\nu_1+\nu_2+\nu_3$ band, we present in **Fig. 11** a direct comparison between the CRDS spectrum in a section of the *P*- branch and a simulation based on our combined list. Note the presence of a high number of unassigned narrow lines in the displayed interval which are believed to be belong to ozone rovibrational bands which remain to be identified.

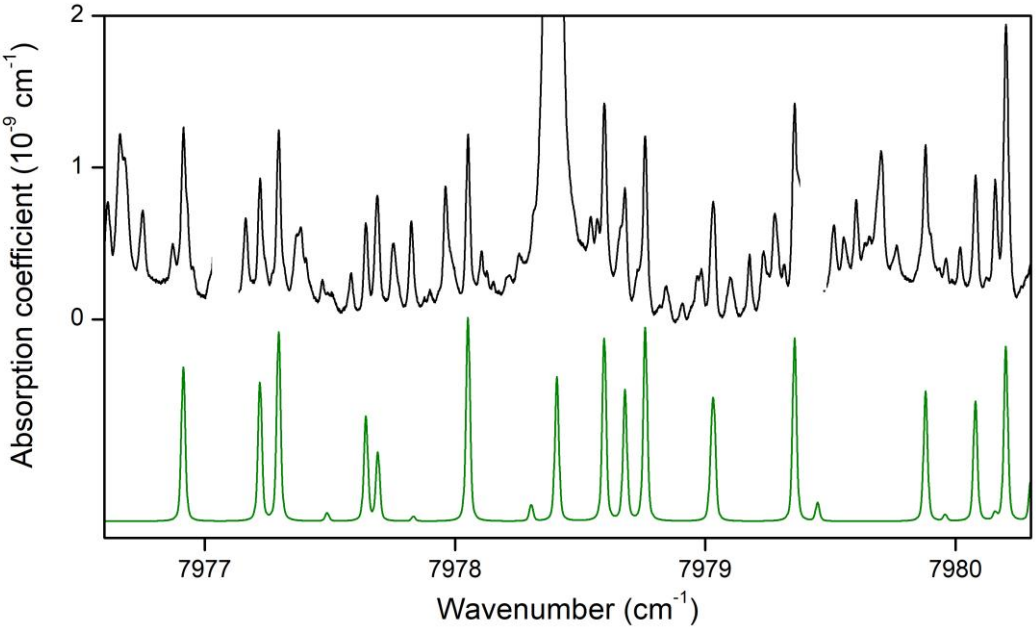

FIG. 11. Example of spectrum comparison in the region of P branch of the $6\nu_1+\nu_2+\nu_3$ band of $^{16}O_3$. *Upper panel*: CRDS spectrum including the $6\nu_1+\nu_2+\nu_3$ band, impurity lines (water and CO_2) and additional unidentified lines probably due to ozone. *Lower panel*: simulation limited to transitions reaching experimentally determined upper levels with intensities computed from EH and EDM (Table I) and line positions empirically corrected.

IV. SUMMARY AND DISCUSSION

The exceptional sensitivity of the CRDS experimental setup used in the present work has allowed for the detection and analysis of two extremely weak combinations bands of $^{16}O_3$ above 7900 cm^{-1}, with upper states involving up to ten vibrational quanta. In **Fig. 12**, their line lists have been gathered with the HITRAN2016 list and previous CRDS data, below and above 5850 cm^{-1}, respectively. The two newly reported bands are the highest energy bands reported so far. Their intensity is smaller by nine orders of magnitude compared to the fundamentals bands [41,81]. The line lists provided in Supplementary Materials contains Einstein coefficients of these transitions involving large changes in vibrational quantum numbers that can have implications for modelling the ozone dynamics including non-LTE processes [17].

The assignment of 432 transitions of the $\nu_1+6\nu_2+3\nu_3$ and $6\nu_1+\nu_2+\nu_3$ bands allowed us to determine 240 upper state vibration-rotation levels between 7969 and 8277 cm^{-1} (see **Fig. 13**). This represents the highest so far obtained experimental set of rotationally resolved data up to J_{max} = 25 in the range 93.1-96.6 % of the dissociation threshold, D_0 (The highest energy level is [J, K_a, K_c]= [25, 3, 22] with an energy of 8277.3 cm^{-1}). As anticipated from previous studies [], the conventional effective Hamiltonians fits based on semi-rigid rotor approximation, including centrifugal distortion and empirical resonance coupling terms, do not reach experimental accuracy in this range. This is consistent with the general trend of *rms* deviations of EH fits plotted in Fig. 7 of Ref. [42]. However, most of our assignments are supported by GSCD relations involving transitions from *P*- , *Q*- and *R*-branches providing thus reliable information independently of a shortcoming of EH models. The consistence of the energy level values determined from different lines (see **Table I**) indicates that the average uncertainty of our energy set is better than 10^{-3} cm^{-1} which is better than achieved in some lower energy ranges.

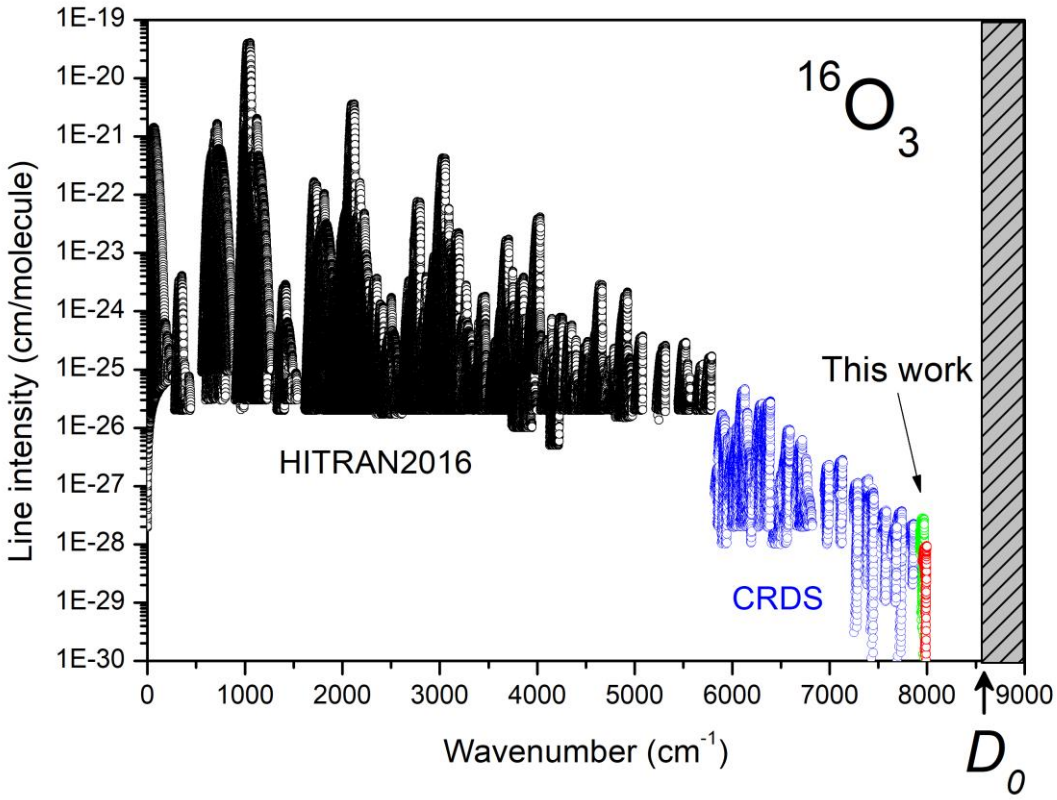

FIG. 12. Overview of the line lists of the analyzed rovibrational bands of $^{16}O_3$. Up to 5850 cm^{-1}, line list provided by the HITRAN2016 database (black circles) is reproduced. The CRDS data of Refs. [] cover the 5850-7900 cm^{-1} region (blue circles) while the most excited bands above 7900 cm^{-1} are the $\nu_1+6\nu_2+3\nu_3$ band (green) and $6\nu_1+\nu_2+\nu_3$ (red) bands studied in this work. The dissociation threshold (8520 cm^{-1} [51]) is indicated.

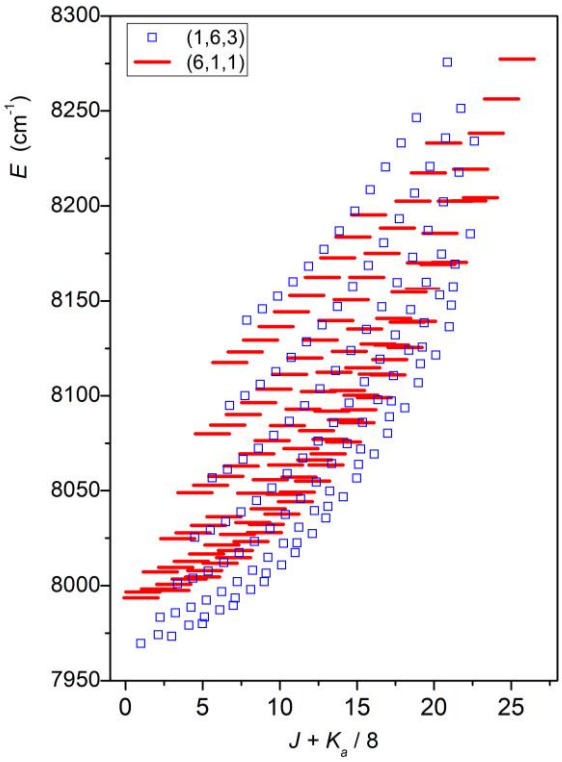

FIG.13. Experimentally determined vibration-rotation levels of (1,6,3) and (6,1,1) vibrational states of $^{16}O_3$ as a function of the rotational quantum numbers J and K_a.

The derived experimental band centres and A_V, B_V, C_V rotational constants provide valuable information for comparison with *ab initio* calculations. Predicted values of A_V, B_V, C_V were critical for the rovibrational assignments, as they essentially determine the distance between the band centres and the band heads. The overall agreement (**Table IV**) is almost as good as for bands at lower energy [42,52,63,64] confirming the validity of the *ab initio* PES of Ref. [26] in this very high energy range.

Table IV. Comparison of experimentally determined band centers and upper state rotational constants with *ab initio* predictions using two methods of variational calculations [26].

		1-well (C_{2V}) [26]		3-wells (D_{3h}(M)) [30,31]	
Upper state	Exp. (TW)	*ab initio*	Exp.-Calc.	*ab initio*	Exp.-Calc.
(1,6,3)	7968.78	7971.69	-2.91	7971.12	-2.34
A_v	3.448	3.472	-0.023	3.442	0.006
B_v	0.402	0.396	0.006	0.388	0.014
C_v	0.341	0.348	-0.007	0.344	-0.003
(6,1,1)	7992.83	7991.66	1.17	7991.66	1.17
A_v	3.414	3.407	0.006	3.411	0.003
B_v	0.417	0.416	0.002	0.410	0.007
C_v	0.369	0.366	0.002	0.363	0.006

Note:
All values are given in cm^{-1}. TW = This work.
1-well (C_{2V}): variational calculations in one potential well of C_{2v} point group.
3-wells (D_{3h}(M)): variational calculations in three potential wells of D_{3h}(M) symmetry.
In both variational predictions the same *ab initio* PES of [26] has been used.

It is instructive to examine in more details the comparison for the band centres E_V with *ab initio* predictions using two types of recent variational calculations. It is well-known that the equilibrium geometry of ozone molecule corresponds to ($r^{(e)}_{13}$ = 4.1a_0) > ($r^{(e)}_{12}$ = $r^{(e)}_{23}$ = 2.4 a_0), where low case indices stand for $O_{(1)}$ and $O_{(3)}$ edge oxygen atoms and $O_{(2)}$ for the central oxygen atom making ozone an asymmetric top molecule of C_{2V} point group (a_0 is the Bohr radius). The first variational method [26] was constrained to bound levels calculations within one potential well of the "open-state" configuration belonging to C_{2V} point group, which corresponds to the geometrical sector (r_{12} <r_{13}> r_{23}). The other variational method [30,31] is based on a full account of the permutation symmetry among three identical oxygen nuclei, corresponding to D_{3h}(M) group using symmetry adapted hyper-spherical coordinates [82-84]. The used PES was the same in both calculations with the same shape in the transition state range and towards the dissociation limit, just symmetrised in three sectors of nuclear geometri*es* (r_{12}<r_{13}>r_{23}; r_{13}<r_{12}>r_{23}; *and* r_{12}<r_{23}>r_{13}). This gives rise to three identical potential wells separated by barriers. For all bound states of ozone experimentally measured up to now [42,50,54-63] both theoretical approaches produced identical energy values (differences less than 0.01 cm^{-1}) [26,30]. The first notable difference of 0.57 cm^{-1} is predicted for the (B_1,89) vibration level assigned to (υ_1,υ_2,υ_3) = (1,6,3), observed in this work. The discrepancies between the 1-well and 3-wells calculations, increasing towards D_0, can be explained by interactions among the three potential wells, which had not been experimentally evidenced yet. Though at this stage of the study it is too early to claim for an experimental proof of such coupling effects, the comparison (Table IV) with our experimental value for the level (1,6,3) gives a hint that the 3-wells predictions go to the right direction slightly diminishing the *ab initio* error by more than 20%. A particular sensitivity of the (1,6,3) state to this interaction is supported by vibrational dynamics considerations: a simultaneous excitation of the high bending $6\nu_2$ and asymmetric stretching $3\nu_3$ modes points in the direction towards another potential well making the molecule more floppy. Such effect is not expected in the (6,1,1) state where mostly quite rigid symmetric stretch vibrations $6\nu_1$ are activated (The 1-well and 3-wells *ab initio* values are identical – see **Table IV**).

The effects of the interactions among the three potential wells should be confirmed by further observations above 8000 cm^{-1}. Besides the experimental challenge, an extension of the analyses towards D_0 will require accurate theoretical predictions both for hot bands in electronic transitions $^3A_2(000)–X(V_1V_2V_3)$ and *ab initio* intensities of rovibrational bands with large variation of vibration quantum numbers, which up to now were limited by ΔV_{max} =6 [71]. A study of qualitative changes of vibrational modes [85] on global *ab initio* PESs will be helpful for band assignments as well as for the account of non-adiabatic interactions of electronic states [20-22,29] near the dissociation asymptote.

Acknowledgements
The supports from CNRS (France) in the frame of the International Research Project SAMIA with IAO-Tomsk and from the Russian Science Foundation (project RNF-19-12-00171) are acknowledged. We are grateful to S. Tashkun (IAO Tomsk, Russia) for collaboration in software development.